Nacre morphology and chemical composition in Atlantic winged oyster *Pteria colymbus* (Röding, 1798)

Pablo Santana [1], **Dalila Aldana Aranda** [Corresp. 1]

[1] Departamento de Recursos del Mar, Centro de Investigación y de Estudios Avanzados del Instituto Politécnico Nacional, MERIDA, Yucatán, México

Corresponding Author: Dalila Aldana Aranda
Email address: daldana@cinvestav.mx

The microstructure and nanostructure of nacre in *Pteria colymbus* were studied with high-resolution field emission scanning electron microscopy (FESEM). The tablets were found to be flat and polyhedral with four to eight sides, and lengths ranging from 0.6 to 3.0 µm. They consisted of nanocrystals 41 nm wide, growing in the same direction. X-ray diffraction showed the crystals to be mineral phase aragonite, which was confirmed by Raman spectroscopy. Fourier transform infrared spectroscopy identified a band at 1786.95 cm^{-1} attributed to carboxylate (carbonyl) groups of the proteins present in the organic matrix as well as bands characteristic of calcium carbonate. X-ray fluorescence showed the nacre to contain 98% calcium carbonate, as well as minor elements (Si, Na, S and Sr) and trace elements (Mg, P, Cu, Al, Fe, Cl, K and Zn).

Nacre morphology and chemical composition in Atlantic winged oyster *Pteria colymbus* (Röding, 1798)

Pablo Santana-Flores[1], Dalila Aldana Aranda[1]

[1]Departamento de Recursos del Mar, Centro de Investigación y de Estudios Avanzados, Mérida, Yucatán, México

Corresponding Author:
Dalila Aldana Aranda[1]
Laboratorio de Biología y Acuacultura de Moluscos, Km 6 antigua Carretera a Progreso S/N Cordemex, Mérida, Yucatán, 97310, México
Email address: daldana@cinvestav.mx

Abstract

The microstructure and nanostructure of nacre in *Pteria colymbus* were studied with high resolution field emission scanning electron microscopy (FESEM). The tablets were found to be flat and polyhedral with four to eight sides, and lengths ranging from 0.6 to 3.0 μm. They consisted of nanocrystals 41 nm wide, growing in the same direction. X-ray diffraction showed the crystals to be mineral phase aragonite, which was confirmed by Raman spectroscopy. Fourier transform infrared spectroscopy identified a band at 1786.95 cm^{-1} attributed to carboxylate (carbonyl) groups of the proteins present in the organic matrix as well as bands characteristic of calcium carbonate. X-ray fluorescence showed the nacre to contain 98% calcium carbonate, as well as minor elements (Si, Na, S and Sr) and trace elements (Mg, P, Cu, Al, Fe, Cl, K and Zn).

Introduction

Mollusk shells are mineralized tissues that fulfill structural functions (Addadi, Raz & Weiner, 2003). In all three main mollusk classes (Cephalopoda, Gastropoda and Bivalvia) the shell consists of stratified layers, each with a unique mineral composition (Dauphin & Denis, 2000). Shell-forming crystals are organized on these layers according to different configurations which define a shell's microstructures. Specific microstructures are characteristic of calcite (i.e., prismatic, foliate) and aragonite (i.e., nacre, laminar cross). Secreted polymorph type and microstructural types are used to characterize large mollusk groups, particularly the bivalves.

Nacre is the most studied aragonitic microstructure and is widely distributed in mollusks (Towe & Hamilton, 1967). Its stratified microstructure gives mother-of-pearl its luster and provides excellent mechanical properties. Nacre has been of great interest to the pearl industry, making it one of the most studied hard tissues (Wang et al., 2013). Because it is osteoconductive and biodegradable, interest has increased recently in technological applications related to nacre, such as the manufacture of bio-inspired super-resistant materials and clinical implants (Tang et al., 2003; Oaki & Imai, 2005).

In each of the three main mollusk classes (Gastropoda, Cephalopoda and Bivalvia) nacre exhibits specific growth patterns and mechanisms. In Gastropoda, for example, the aragonite nanocrystals in the nacre are stacked in towers and their c axes are aligned. However, they have a composite cross laminar arrangement, and a third hierarchical order of flat aragonite fibers from 50 to 100 nm thick, 300 nm wide and a few micrometers long (Romana et al., 2013). In the nautilus (Cephalopoda), nacre exhibits a mixed behavior with simultaneous growth in towers and terraces occurring in adjacent locations (Saunders & Landman, 2010). Nacre in the Bivalvia has terraced growth and the three axes of crystals are co-oriented. The order Pterioidae has shells that are unequal, monomyary, and not equilateral; the right valve is generally less convex than the left (Wada & Tëmkin, 2008; Cummings & Graf, 2015). Their shells are formed by superposition of an outer organic layer, the periostracum, a prismatic layer and the inner nacreous layer (Kennedy, Taylor & Hall, 1969).

Nacre is a biomineral consisting (by weight) of 95% aragonite ($CaCO_3$) with the remaining 1 to 5% being organic matrix(Zhang & Li, 2012). Its microstructure is one of layered “brick” (aragonite tablets) and “mortar” (protein-polysaccharide matrix). This structure provides nacre with twice the strength and up to 1000 times the toughness of its constituent components alone (Li et al., 2004; Veis & Dorvee, 2013; Morris et al., 2016). Individual nacre tablets have a nanoscale structure based on aragonite nanograins, nanoblocks and nanofibers (Wang et al., 2013). Nanoscale structural organization differs between bivalve mollusks, resulting in different tablet forms at growth completion.

Better understanding of the composition and hierarchy of biological system microstructures is key in the search for new materials and provides deeper insight into evolutionary processes (Jáuregui-Zúñiga et al., 2003; Oaki & Imai, 2005; Wang et al., 2013; Nakamura Filho et al., 2014; Wegst et al., 2015). The present study objective was to analyze the micro- and nanostructure of *P. colymbus*

nacre with scanning electron microscopy, and its chemical composition with x-ray diffraction, X-ray fluorescence spectrometry, Fourier transform infrared spectrometry and Raman spectroscopy.

Materials & Methods

Shells of *Pteria colymbus* were collected in the Alacranes Reef, in the state of Yucatán, Mexico. They were placed in a soap solution, cleaned, and stored at 4 °C for 48 hours. To remove the inorganic and biogenic matter from shells was cleaned by ultrasound with a soap solution for five minutes. (Ky, Lo & Planes, 2017). Six 1 cm^2 samples were cut from the shells using a 32 mm-diameter diamond disc. Samples were washed again by ultrasound for five minutes and dried at 65 °C for three hours (Ren et al., 2009; Xu & Zhang, 2015).

Nacre tablet morphology was characterized with a JEOL 7600F ultra high resolution field emission scanning electron microscope (FESEM). Samples were coated with Au/Pd and processed at a 1-30 kV acceleration voltage (Ren et al., 2009; Liu & Li, 2015).

For the chemical analysis, a 1 cm^2 nacreous layer sample was separated from the shell with the help of a rotary tool at 2000 RPM. The sample was always kept immersed in water at room temperature. The sample was cleaned by ultrasound with a soap solution for five minutes and dried at 65 °C for three hours. Subsequently, it was placed in aluminum sample holders for analysis in the diffractometer (Bruker D8) using monochromatic CuKa radiation. The XRD patterns were collected at 20 to 90 ° (2Θ) in 0.02 ° steps with a 0.96 s count time interval. The resulting diffraction patterns were compared with the card for aragonite (PDF no. 000411475) from the crystallographic records of the International Center for Diffraction Data (ICDD) database (Weiner & Traub, 1980; de Paula & Silveira, 2009; Heinemann et al., 2011).

To analyze the nacre by Fourier transform infrared spectrometry (FTIR) analysis, the nacre layer from the shell was separated with a rotary tool at 2000 RPM. The sample was ultrasonically cleaned with a soap solution and dried at 65 °C for 3 hours. The sample was ground in an agate mortar to give the appearance of a fine powder and then dried at 65 °C for 3 hours. Tablets were prepared with 0.5 mg of nacre powder and 200 mg of KBr. Infrared analyzes were run at a 4 cm resolution in two wave ranges: 400-4000 cm^{-1} and 550-4000 cm^{-1}. The analyzes were done in reflectance mode on a FTIR spectrometer with Bruker accessory (EQUINOX 5). Spectra were automatically corrected for water, carbon dioxide and the KBr background (Monarumit et al., 2015; Zhang et al., 2016; Cardoso et al., 2016).

Chemical analyses were also done using the semi-quantitative method of X-ray fluorescence spectrometry (XFR) with wave dispersion in a spectrometer (Bruker S4 Pioneer) with a 4kW excitation source. A vacuum scan was done of 71 elements (11Na-92U) using an RX tube with Rh anode, 25 to 60 kV excitation voltage, and a 0.46 dg collimator with a 34 mm mask. Data was interpreted with the Spectra Plus software. Quantification of $CaCO_3$ was done with an ignition loss analysis at 950 °C for one hour (Shi et al., 2018).

The $CaCO_3$ crystalline phase was identified using a Raman spectrometer with focal point (WITEC Alpha 300) (λexc = 488 and 785 nm; acquisition time 10 s; resolution 10 cm^{-1}).

Results

Microstructure and nanostructure

The shell of *P. colymbus* consists of a prismatic and an aragonitic layer clearly divided by a slight change in color (Figure 1, indicated by arrow and BL symbol). The FESEM analysis identified an organic hydrogel on some tablets in different layers (Figure 2a). In another growth section of the pearlescent layer small growing crystals were observed to be fusing with each other (Fig. 2b). The tablets form a uniform sheet at the point where the next layer begins to grow and in some cases the tablets fuse with higher layers (Figure 2c). Mature tablets are four to eight-sided, 0.6 to 3.0 µm in length, and can be fused (Figure 2d).

Cross sections of the nacre tablets showed a nanostructure in which the first layer of deposited nacre consisted of packed nanocrystals forming tablets. These were longer than in the upper layers and their growth was perpendicular to the surface (Figure 3a). Crystals in initial growth stages were observed in a section close to the prismatic layer (Figure 3b). In the intermediate section of the shell all the deposited nacre layers contained tablets composed of a package of crystals fused in the “brick and mortar” arrangement typical of species in the Pteriidae family. Average tablet thickness was 385 nm (SD = 0.069) (n = 187) with a range of 200 to 530 nm (Figure 3c). The nanocrystals were uniformly oriented perpendicular to shell surface, have a 41 nm (SD = 9.43) (n = 24) average width, and a length range of 24 to 69 nm (n = 24) (Figure 3d).

Chemical analysis

The XRD pattern of the nacre layer showed the main reflection to be at 31.05 (2Θ) with two lesser readings at 33.0 (2Θ) and 66.0 (2Θ), both characteristic of aragonite (Figure 4).

The XRF analysis identified aragonite as representing 98.13% of sample weight. Minor elements were Si (0.72%), Na (0.5500%), S (0.2080%), and Sr (0.1042%), and trace elements were Mg (0.0897%), P (0.0485%), Cu (0.0353%), Al (0.0331), Fe (0.0311%), Cl (0.0290%), K (0.0151% and Zn (0.0060%). The nacre's aragonite structure was confirmed in the FTIR analysis (Figure 5). Four bands characteristic of aragonite, corresponding to the CO_3^{2-} ions, were identified: v3 at 1445.96 cm^{-1}; v1 at 1082.72 cm^{-1}; v2 at 856.80 cm^{-1}; and v4 at 699.81-712.52 cm^{-1}. The v4 band corresponds to the planar flexion mode of carbonate vibration and the v1 band to the symmetric stretch mode. The nacre FTIR spectrum revealed lower intensity organic bands; the band at 1786.95 cm^{-1} was attributed to the carboxylate (carbonyl) groups of the acidic proteins in the organic matrix.

The Raman spectroscopy analysis of the nacre surface produced the most intense band at near 1085 cm^{-1} in the aragonite spectra which corresponds to symmetrical stretching mode v1 of the carbonate ion (Figure 6). Low- to medium-intensity bands in the 100-300 cm^{-1} region of the aragonite spectra were due to the translational and rotational modes of lattice vibration. The v4 in the carbonate ion plane bending mode occurred as a doublet with bands between 701 and 705 cm^{-1}.

Discussion

Nacre in *P. colymbus* consists of polygonal tablets with four to eight sides, a morphological characteristic also present in species such as *Pinctada maxima*, *Pinctada radiata* and *Pinctada fucata* (Wang et al., 2001; Bellaaj-Zouari et al., 2011; Zhang, Xie & Yan, 2019). However, tablet length differs between species in the Pteriidae family. In *P. colymbus*, length ranges from 0.6 to 3.0 μm, whereas in *P. radiata* it ranges from 4.0 to 5.0 μm (Bellaaj-Zouari et al., 2011), and in *P. margaritifera* from 5.0 to 10.0 μm (Rousseau et al., 2009).

Morphological differences in pearl oysters can be seasonal or intrinsic to each species (Wada, 1972). Intrinsic differences are due to genetic control of shell mineralogy and any similarities between species can be traced to the Mesozoic/Paleozoic boundary (Kennedy, Taylor & Hall, 1969). Environmental factors such as temperature can modify shell structure in different organisms. For instance, shell aragonite percentage in the mussel *Mytilus californianus* decreases from 45% in the spring to 30% in the winter, but only in organisms longer than 15 mm (Kennedy, Taylor & Hall, 1969). Slower nacre deposition rates may be in response to reductions in water temperature, probably in winter, combined with lower food availability (Taylor & Strack, 2008).

In another example, in *P. fucata* nacre growth and thickness respond to tablet thickness which is 324 nm when water temperature is highest, during August, but only 224 nm when it is lower, in December (Muhammad et al., 2017). Decreases in tablet thickness favor light iridescence of the nacre surface which is why pearl producers harvest pearls when sea water temperature decreases (Suzuki & Nagasawa, 2013).

The tablets in *P. colymbus* shell contain nanocrystals ranging in thickness from 24 to 69 nm. This coincides with tablets in *P. maxima* which consist of aragonite nanofibrils from 10 to 30 nm thick (Wang et al. 2012). Tablets in abalone *Haliotis rufescens* shell are built of parallel aragonite nanoparticles (Huang and Li 2012), and its nanostructure is one of polygonal cobble-like grains (~32 nm) within individual aragonite tablets (Li et al. 2004). The shell of *P. fucata* contains nanoblocks from 20 to 180 nm long (Oaki & Imai, 2005).

In each species formation of the aragonite nanoparticles in nacre tablets is regulated by organic matrix characteristics (Dauphin and Denis, 2000, Kim et al. 2006). The distribution of organic macromolecules during crystal growth is important since these regulate crystal size, shape, and orientation (Okumura et al., 2012; Shtukenberg, Ward & Kahr, 2017).

In *Tellinella asperrima* shells, the crystallographic orientation of aragonite between nacre and nacre powder (ground at 45 μm) was investigated. It was found that there is a strong preferential crystallographic orientation of the diffraction peak at the angle $2\Theta = 31.03\ ^\circ$ of the intact nacre, simultaneously two other peaks with weak preferential orientations were found (Ren et al. 2000). In this work, it was found that the X-ray diffraction pattern of the nacre of *P. colymbus* is very similar to the intact nacre of *T. asperrima*. Presenting greater intensity in the main diffraction peak and the same intensity in the minor peaks. This preferential crystal orientation of aragonite in nacre is frequently found in biological mineralization and is due to the presence of b-chitin fibrils and the protein polypeptide chains that control crystal growth. (Feng et al 2000).

Calcium carbonate ($CaCO_3$) in the form of aragonite represents 98.13% of the total nacre layer in *P. colymbus* in the present results. The majority presence of aragonite in the shell coincides with other species in the Pteriidae family, such as *P. fucata* (Saruwatari et al., 2009) and *P. margaritifera* (Shi et al., 2018), as well as the mussel *Perna viridis* (Xu & Zhang, 2015). Minor elements are Si, Na, S and Sr, and trace elements are Mg, P, Cu, Al, Fe, Cl, K and Zn. In another study, nacre was found to be composed of calcium carbonate (91.50%) with traces of organic substances (3.83%), residual substances (0.01%) and water (3.97%) (Taylor & Strack, 2008).

These residual substances include Na, Cl and K, as well as traces and other elements such as Ba, Mg, P, Mn, Fe, Al, Cu, Zn, Ag, Hg, Li and Mr. The trace element profile of a nacre reflects water mineral composition in the place where it formed. In biogenic aragonite crystals other elements such as Mn, Mg, Sr, and Ba can substitute for calcium (Gaetani & Cohen, 2006; Chen et al., 2011). Notable differences in the concentration of these elements exist between taxonomic groups, highlighting genetic influence on their incorporation (Carré et al., 2006).

The other elements present in nacre function as precursor ions in nacre formation, as catalysts in proteins and activators of enzymes; they are present in intercrystalline organic macromolecules and the organism's epithelial fluid (Marsh & Sass, 1983; Cho & Jeong, 2011; Marin, 2012).

Conclusions

Nacre composition in *P. colymbus* has high aragonite content and its nanostructure consists of polygonal tablets built of nanocrystals. The present is a preliminary description of *P. colymbus* carapace structure intended as a presentation of the relevant data to date, and a guide for further research.

Acknowledgements

The authors thank Patricia Quintana access to LANNBIO facilities, Dora Huerta, and Daniel Aguilar for assistance with the diffractograms and SEM images. The authors also thank Maria del Socorro Garcia Guillermo, Ixchel Rubí Perez, Ana Elena Muñiz, and Norma Alicia Berlanga, at Cinvestav-Saltillo chemical analysis General Laboratory for her support in carrying out this work.

References

Addadi L, Raz S, Weiner S. 2003. Taking advantage of disorder: amorphous calcium carbonate and its roles in biomineralization. *Advanced Materials* 15:959–970. DOI: 10.1002/adma.200300381.

Bellaaj-Zouari A, Chérif K, Elloumi-Hannachi I, Slimane N, Habib J. 2011. Characterization of mineral and organic phases in nacre of the invasive pearl oyster *Pinctada radiata* (Leach, 1814). *Cahiers de Biologie Marine* 52:337–348.

Cardoso SSS, Cartwright JHE, Checa AG, Sainz-Díaz CI. 2016. Fluid-flow-templated self-assembly of calcium carbonate tubes in the laboratory and in biomineralization: the tubules of the watering-pot shells, Clavagelloidea. *Acta Biomaterialia* 43:338–347. DOI: 10.1016/j.actbio.2016.07.005.

Carré M, Bentaleb I, Bruguier O, Ordinola E, Barrett NT, Fontugne M. 2006. Calcification rate influence on trace element concentrations in aragonitic bivalve shells: evidences and mechanisms. *Geochimica et Cosmochimica Acta* 70:4906–4920. DOI: 10.1016/j.gca.2006.07.019.

Chen T, Yu K, Li S, Chen T, Shi Q. 2011. Anomalous Ba/Ca signals associated with low temperature stresses in porites corals from Daya Bay, northern South China Sea. *Journal of Environmental Sciences* 23:1452–1459. DOI: 10.1016/S1001-0742(10)60606-7.

Cho S-M, Jeong W-G. 2011. Prismatic shell repairs by hemoctyes in the extrapallial fluid of the Pacific Oyster, *Crassostrea gigas*. *The Korean Journal of Malacology* 27:223–228. DOI: 10.9710/kjm.2011.27.3.223.

Cummings KS, Graf DL. 2015. Class Bivalvia. In: *Thorp and Covich's Freshwater Invertebrates*. Elsevier, 423–506. DOI: 10.1016/B978-0-12-385026-3.00019-X.

Dauphin Y, Denis A. 2000. Structure and composition of the aragonitic crossed lamellar layers in six species of Bivalvia and Gastropoda. *Comparative Biochemistry and Physiology Part A: Molecular & Integrative Physiology* 126:367–377. DOI: 10.1016/S1095-6433(00)00213-0.

Gaetani GA, Cohen AL. 2006. Element partitioning during precipitation of aragonite from seawater: a framework for understanding paleoproxies. *Geochimica et Cosmochimica Acta* 70:4617–4634. DOI: 10.1016/j.gca.2006.07.008.

Heinemann F, Launspach M, Gries K, Fritz M. 2011. Gastropod nacre: structure, properties and growth — Biological, chemical and physical basics. *Biophysical Chemistry* 153:126–153. DOI: 10.1016/j.bpc.2010.11.003.

Jáuregui-Zúñiga D, Reyes-Grajeda J, Sepúlveda-Sánchez J, Whitaker JohnR, Moreno A. 2003. Crystallochemical characterization of calcium oxalate crystals isolated from seed coats of

Phaseolus vulgaris and leaves of *Vitis vinifera*. *Journal of Plant Physiology* 160:239–245. DOI: 10.1078/0176-1617-00947.

Kennedy WJ, Taylor JD, Hall A. 1969. Environmental and biological controls on bivalve shell mineralogy. *Biological Reviews* 44:499–530. DOI: 10.1111/j.1469-185X.1969.tb00610.x.

Ky C-L, Lo C, Planes S. 2017. Mono- and polychromatic inner shell phenotype diversity in *Pinctada margaritifera* donor pearl oysters and its relation with cultured pearl colour. *Aquaculture* 468:199–205. DOI: 10.1016/j.aquaculture.2016.10.017.

Li X, Chang W-C, Chao YJ, Wang R, Chang M. 2004. Nanoscale structural and mechanical characterization of a natural nanocomposite material: the shell of red abalone. *Nano Letters* 4:613–617. DOI: 10.1021/nl049962k.

Liu X, Li J. 2015. Formation of the prismatic layer in the freshwater bivalve *Hyriopsis cumingii*: the feedback of crystal growth on organic matrix. *Acta Zoologica* 96:30–36. DOI: 10.1111/azo.12048.

Marin F. 2012. The formation and mineralization of mollusk shell. *Frontiers in Bioscience* S4:1099–1125. DOI: 10.2741/s321.

Marsh ME, Sass RL. 1983. Calcium-binding phosphoprotein particles in the extrapallial fluid and innermost shell lamella of clams. *Journal of Experimental Zoology* 226:193–203. DOI: 10.1002/jez.1402260204.

Monarumit N, Noirawee N, Phlayrahan A, Promdee K, Won-in K, Satitkune S. 2015. Identification of high-luster and lusterless freshwater-cultured pearls by X-ray absorption spectroscopy. *Journal of Applied Spectroscopy* 82:677–680. DOI: 10.1007/s10812-015-0163-3.

Morris JP, Wang Y, Backeljau T, Chapelle G. 2016. Biomimetic and bio-inspired uses of mollusc shells. *Marine Genomics* 27:85–90. DOI: 10.1016/j.margen.2016.04.001.

Muhammad G, Atsumi T, Sunardi, Komaru A. 2017. Nacre growth and thickness of Akoya pearls from Japanese and Hybrid *Pinctada fucata* in response to the aquaculture temperature condition in Ago Bay, Japan. *Aquaculture* 477:35–42. DOI: 10.1016/j.aquaculture.2017.04.032.

267 Nakamura Filho A, Almeida AC de, Riera HE, Araújo JLF de, Gouveia VJP, Carvalho MD de, Cardoso
268 AV. 2014. Polymorphism of $CaCO_3$ and microstructure of the shell of a Brazilian invasive
269 mollusc (*Limnoperna fortunei*). *Materials Research* 17:15–22. DOI: 10.1590/S1516-
270 14392014005000044.
271 Oaki Y, Imai H. 2005. The hierarchical architecture of nacre and its mimetic material. *Angewandte*
272 *Chemie International Edition* 44:6571–6575. DOI: 10.1002/anie.200500338.
273 Okumura T, Suzuki M, Nagasawa H, Kogure T. 2012. Microstructural variation of biogenic calcite with
274 intracrystalline organic macromolecules. *Crystal Growth & Design* 12:224–230. DOI:
275 10.1021/cg200947c.
276 de Paula SM, Silveira M. 2009. Studies on molluscan shells: contributions from microscopic and
277 analytical methods. *Micron* 40:669–690. DOI: 10.1016/j.micron.2009.05.006.
278 Ren F, Wan X, Ma Z, Su J. 2009. Study on microstructure and thermodynamics of nacre in mussel shell.
279 *Materials Chemistry and Physics* 114:367–370. DOI: 10.1016/j.matchemphys.2008.09.036.
280 Romana L, Thomas P, Bilas P, Mansot JL, Merrifiels M, Bercion Y, Aranda DA. 2013. Use of
281 nanoindentation technique for a better understanding of the fracture toughness of *Strombus gigas*
282 conch shell. *Materials Characterization* 76:55–68. DOI: 10.1016/j.matchar.2012.11.010.
283 Rousseau M, Meibom A, Gèze M, Bourrat X, Angellier M, Lopez E. 2009. Dynamics of sheet nacre
284 formation in bivalves. *Journal of Structural Biology* 165:190–195. DOI:
285 10.1016/j.jsb.2008.11.011.
286 Saruwatari K, Matsui T, Mukai H, Nagasawa H, Kogure T. 2009. Nucleation and growth of aragonite
287 crystals at the growth front of nacres in pearl oyster, *Pinctada fucata*. *Biomaterials* 30:3028–
288 3034. DOI: 10.1016/j.biomaterials.2009.03.011.
289 Saunders WB, Landman NH (eds.). 2010. Nautilus: the biology and paleobiology of a living fossil,
290 Reprint with additions. Dordrecht: Springer Netherlands. DOI: 10.1007/978-90-481-3299-7.

291 Shi L, Wang Y, Liu X, Mao J. 2018. Component analysis and identification of Black Tahitian cultured
292 pearls from the oyster *Pinctada margaritifera* using Spectroscopic Techniques. *Journal of*
293 *Applied Spectroscopy* 85:98–102. DOI: 10.1007/s10812-018-0618-4.
294 Shtukenberg AG, Ward MD, Kahr B. 2017. Crystal growth with macromolecular additives. *Chemical*
295 *Reviews* 117:14042–14090. DOI: 10.1021/acs.chemrev.7b00285.
296 Suzuki M, Nagasawa H. 2013. Mollusk shell structures and their formation mechanism. *Canadian*
297 *Journal of Zoology* 91:349–366. DOI: 10.1139/cjz-2012-0333.
298 Tang Z, Kotov NA, Magonov S, Ozturk B. 2003. Nanostructured artificial nacre. *Nature Materials*
299 2:413–418. DOI: 10.1038/nmat906.
300 Taylor J, Strack E. 2008. Pearl oroduction. In: *The Pearl Oyster*. Elsevier, 273–302. DOI: 10.1016/B978-
301 0-444-52976-3.00008-5.
302 Towe KM, Hamilton GH. 1967. Ultrastructure and inferred calcification of the mature and developing
303 nacre in bivalve mollusks. *Calcified Tissue Research* 1:306–318. DOI: 10.1007/BF02008102.
304 Veis A, Dorvee JR. 2013. Biomineralization mechanisms: a new paradigm for crystal nucleation in
305 organic matricies. *Calcified tissue international* 93:307–315. DOI: 10.1007/s00223-012-9678-2.
306 WADA K. 1972. Nucleation and growth of aragonite crystals in the nacre of bivalve molluscs.
307 *Biomineralization* 6:141–159.
308 Wada KT, Tëmkin I. 2008. Chapter 2 - Taxonomy and Phylogeny. In: Southgate PC, Lucas JS eds. *The*
309 *Pearl Oyster*. London: Elsevier, 37–75. DOI: 10.1016/B978-0-444-52976-3.00002-4.
310 Wang RZ, Suo Z, Evans AG, Yao N, Aksay IA. 2001. Deformation mechanisms in nacre. *Journal of*
311 *Materials Research* 16:2485–2493. DOI: 10.1557/JMR.2001.0340.
312 Wang S-N, Yan X-H, Wang R, Yu D-H, Wang X-X. 2013. A microstructural study of individual nacre
313 tablet of *Pinctada maxima*. *Journal of Structural Biology* 183:404–411. DOI:
314 10.1016/j.jsb.2013.07.013.
315 Wegst UGK, Bai H, Saiz E, Tomsia AP, Ritchie RO. 2015. Bioinspired structural materials. *Nature*
316 *Materials* 14:23–36. DOI: 10.1038/nmat4089.

317 Weiner S, Traub W. 1980. X-ray diffraction study of the insoluble organic matrix of mollusk shells. *FEBS*
318 *Letters* 111:311–316. DOI: 10.1016/0014-5793(80)80817-9.
319 Xu J, Zhang G. 2015. Unique morphology and gradient arrangement of nacre's platelets in green mussel
320 shells. *Materials Science and Engineering: C* 52:186–193. DOI: 10.1016/j.msec.2015.03.051.
321 Zhang G, Li X. 2012. Uncovering aragonite nanoparticle self-assembly in nacre—A natural armor.
322 *Crystal Growth & Design* 12:4306–4310. DOI: 10.1021/cg3010344.
323 Zhang R, Xie L, Yan Z. 2019. *Biomineralization mechanism of the pearl oyster, Pinctada fucata*.
324 Singapore: Springer Singapore. DOI: 10.1007/978-981-13-1459-9.
325 Zhang N, Yang S, Xiong L, Hong Y, Chen Y. 2016. Nanoscale toughening mechanism of nacre tablet.
326 *Journal of the Mechanical Behavior of Biomedical Materials* 53:200–209. DOI:
327 10.1016/j.jmbbm.2015.08.020.
328
329

Figure 1

Scanning electron microscopy (SEM) image of the cross-section of *Pteria colymbus* (Mollusca, Bivalvia) shell.

General view of pearl oyster *Pteria colymbus* (Mollusca, Bivalvia) shell showing the prismatic layer (PL) at the lower end, followed by the interface zone (BL) and the nacreous layer (NL) at the top. Middle zone of the nacreous layer (IL).

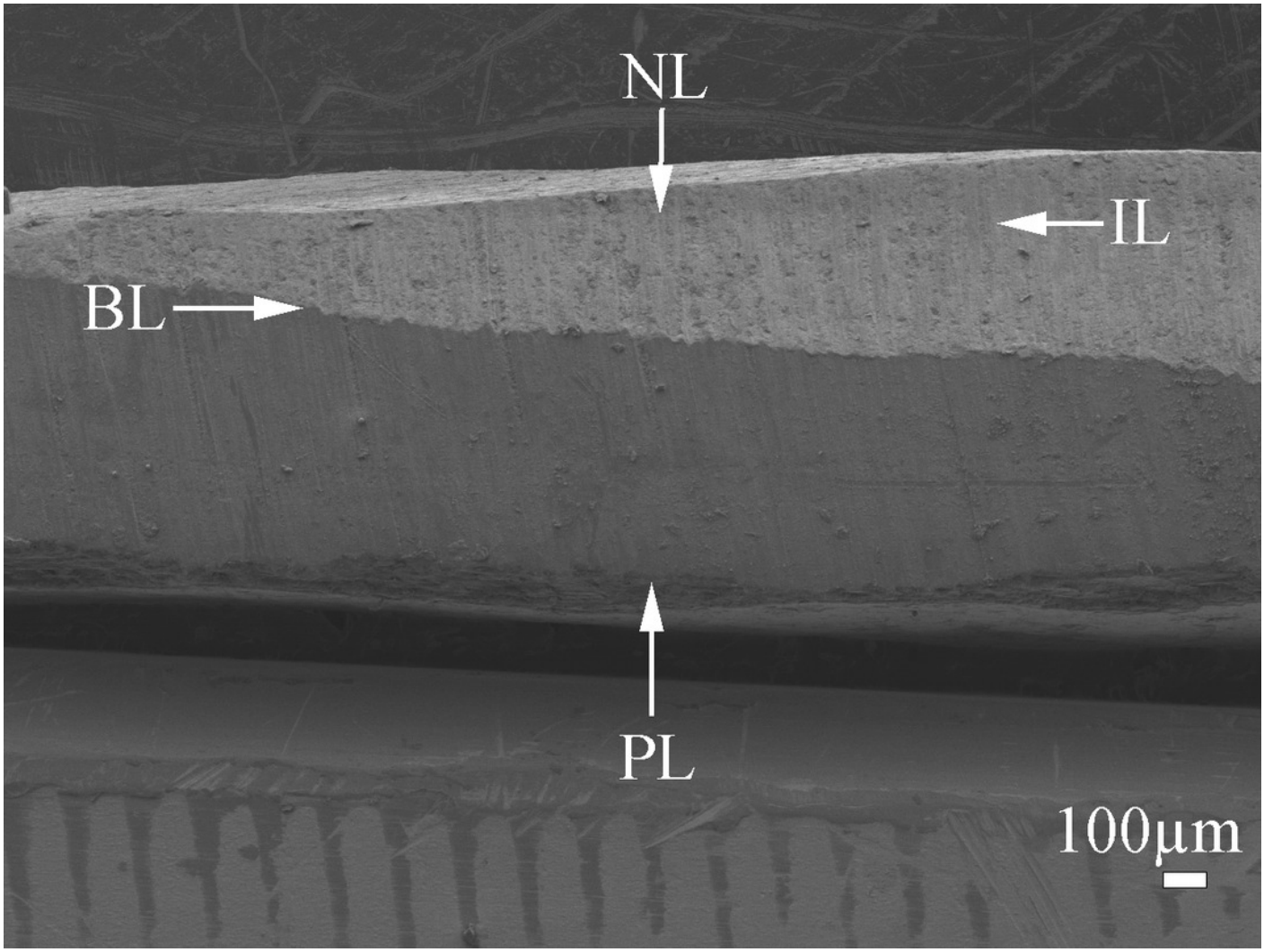

Figure 2

Scanning electron microscopy (SEM) view of the inner surface of the *Pteria colymbus* (Mollusca, Bivalvia) shell.

Microstructure of the nacreous tablets in the inner surface of the *Pteria colymbus* shell. The sample did not receive any polishing and etching treatment. (a) detail of the inner surface of the shell showing recently formed nacre tablets and traces of the hydrogel (arrow) responsible for the formation of the nacre tablets. (b) Detail showing the first stages of nacre crystal formation. Crystal enveloped by organic matrix (★). Crystal in an advanced stage of formation merging with neighboring crystals (✺). (c) Section showing the two different layers of nacre growth merging through a hexagonal-shaped tablet (arrow). (d) Detail of the last layer of nacre showing the different geometries of the nacre tablets. tablet with the minimum number of sides for this species with only 5 µm in length (★). Tablet fused with others with no apparent pattern, which is 40 µm long (✺).

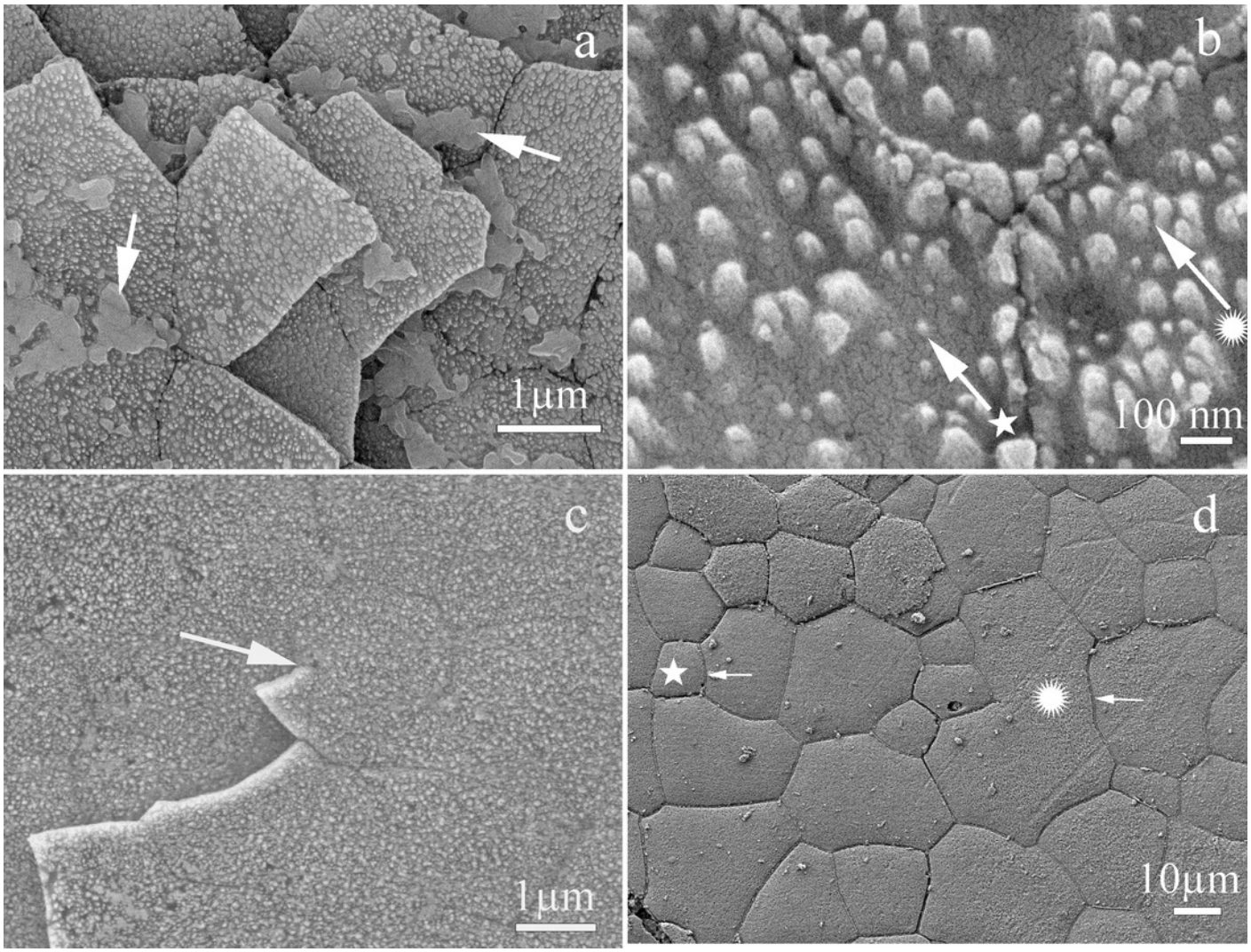
a
1μm
b
100 nm
c
1μm
d
10μm

Figure 3

Scanning electron microscope view of the transverse section of *Pteria colymbus* (Mollusca, Bivalvia) shell.

Microstructure of the first and middle nacre layers in the shell of *Pteria colymbus*. (a) Interface zone of the prismatic and nacreous layers. The first layer of nacre crystals has a growth direction perpendicular to the surface (Arrow). The crystals have a greater length compared to the subsequent layers. The next three nacre layers (NL) have better organization and uniform size. (b) Detail of the nacre crystals (NL) in the first stage of growth. The presence of organic hydrogel (H) is observed, which is covering the prismatic layer (PL). (c) Middle zone of the nacre layer. All nacreous layers contain tablets composed of fused individual crystals. The typical brick and mortar formation, typical of bivalve mollusks (represented by white lines) is observed. The average thickness of the tablets was 385 nm (SD = 0.069). (d) Detail of the nacreous layers in the middle zone. The uniform shapes of the tablets are observed, the crystals that make up the tablets show an early stage of growth (★). Crystals merging from the center in the previous layer (✺). the crystals have a mean width of 41 nm (SD = 9.43).

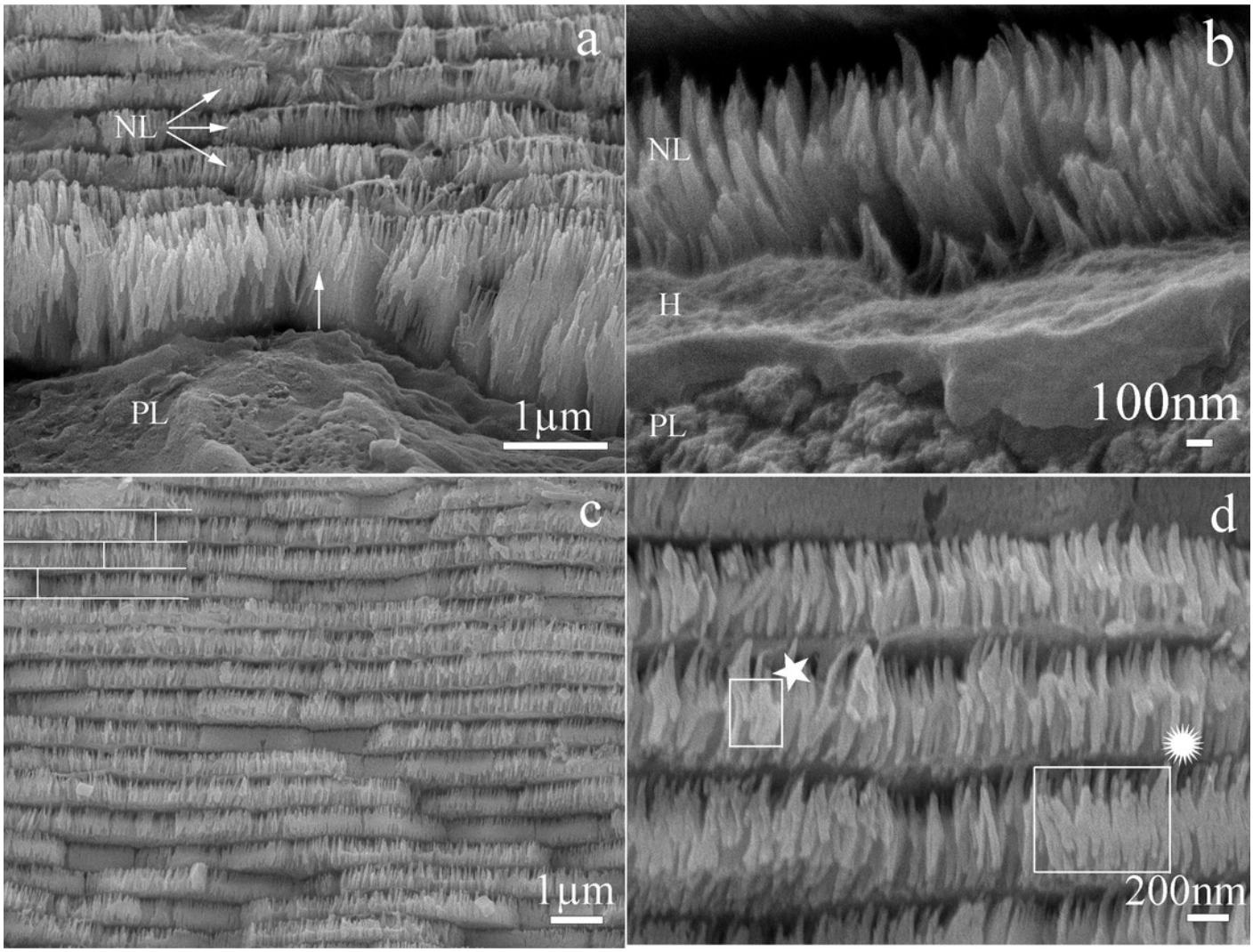
a
NL
PL
1μm
b
NL
H
PL
100nm
c
1μm
d
200nm

Figure 4

X-ray diffraction pattern (XRD) of *Pteria colymbus* (Mollusca, Bivalvia) nacre sample.

The stronger diffraction peak of aragonite in nacreous layer of *Pteria colymbus* is scanning angle 2θ = 31.05°. Red bars represent the Aragonite pattern from PDF 041-1475. (For interpretation of the references to color in this figure legend, the reader is referred to the web version of this article).

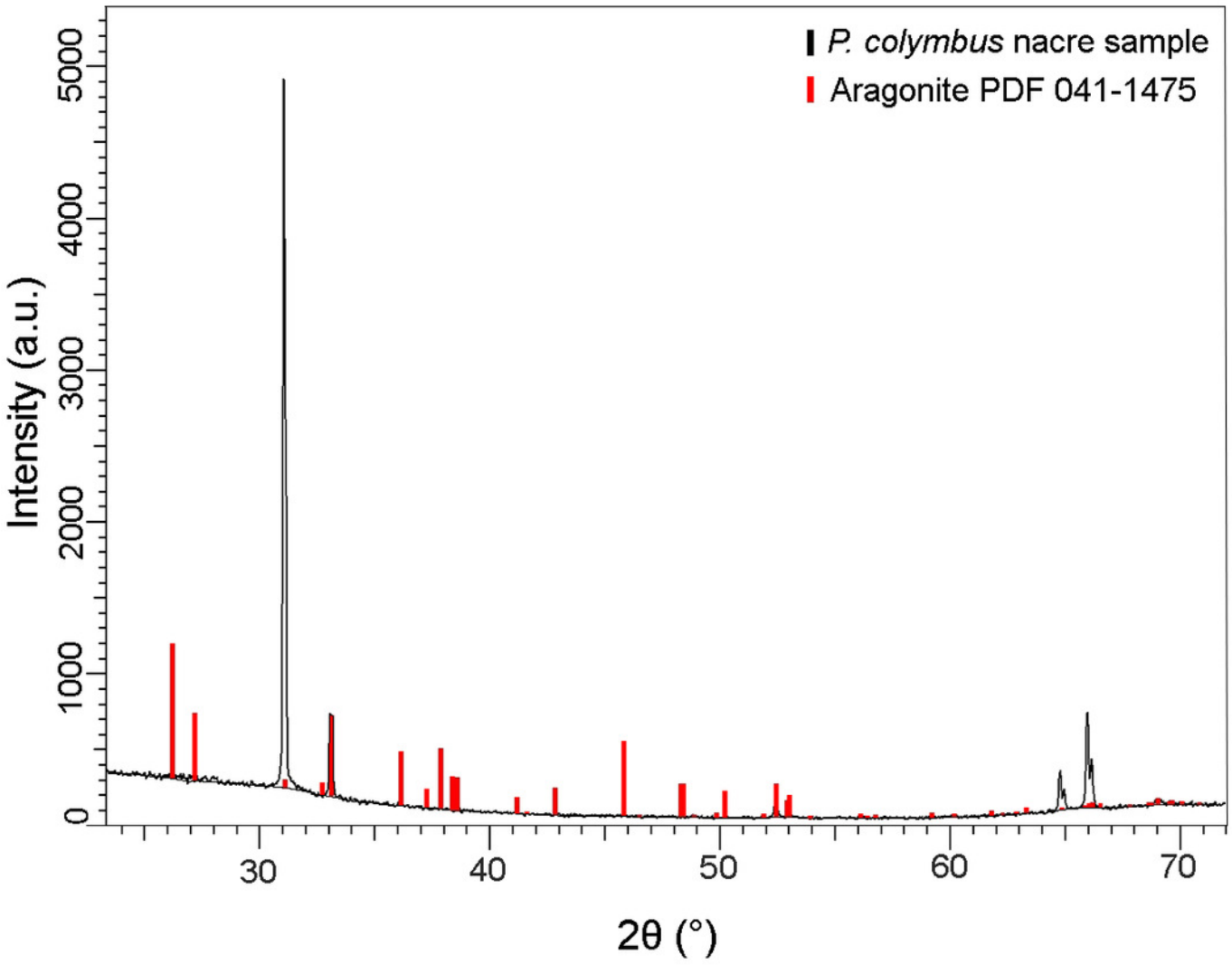

Figure 5

Fourier transform infrared spectrometry (FTIR) spectrum of *Pteria colymbus* (Mollusca, Bivalvia) nacre powder.

The nacre powder sample of *Pteria colymbus* displays a characteristic symmetric carbonate stretching vibration (v1) at 1082.72 cm^{-1} and a carbonate out-of-plane bending vibration (v2) at 856.80 cm^{-1}. The v4 band at 699.81-712.52 cm^{-1} corresponds to the planar flexion mode of carbonate vibration.

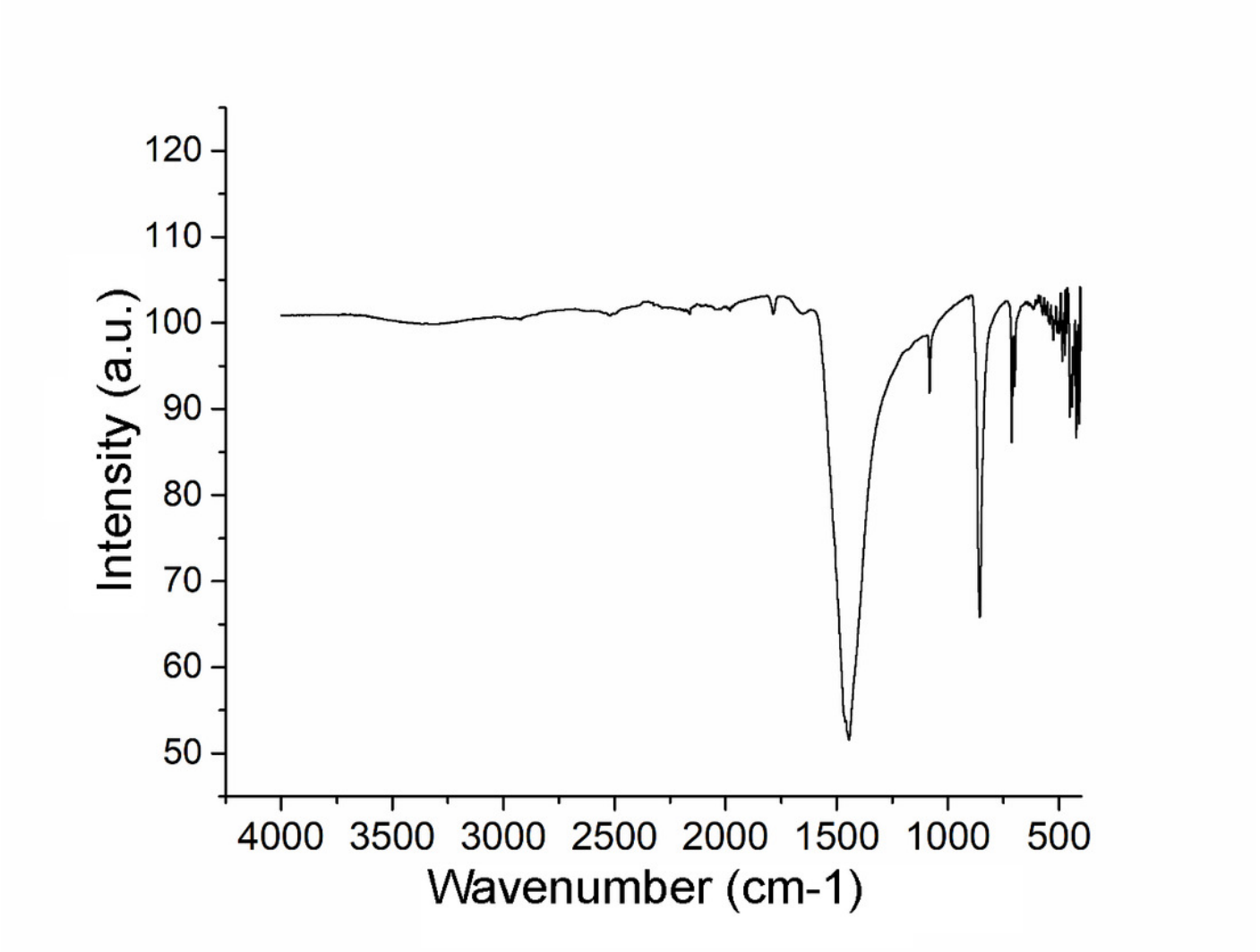

Figure 6

Raman spectra of the *Pteria colymbus* (Mollusca, Bivalvia) nacre layer sample.

The nacreous layer of *Pteria colymbus* shows an intense band at near 1085 cm^{-1} that corresponds to the symmetrical stretching mode of the carbonate ion. Low- to medium-intensity bands in the 100-300 cm^{-1} region were due to the translational and rotational modes of lattice vibration. The carbonate ion plane bending mode occurred as a band between 701 and 705 cm^{-1}.